Electron density distribution in hexagonal cobalt: A γ-ray diffraction study

W. Jauch
Helmholtz-Zentrum Berlin für Materialien und Energie, Glienicker Str. 100, D-14109 Berlin, Germany

M. Reehuis
Max-Planck-Institut für Festkörperforschung, Heisenbergstr. 1, D-70569 Stuttgart, Germany

(Received 28 May 2009; revised manuscript received 10 August 2009; published 25 September 2009)

The electron density distribution of ferromagnetic hexagonal cobalt is studied at room temperature using high-quality single-crystal diffraction data measured up to $\sin\theta/\lambda=1.9$ Å^{-1} with 316.5 keV gamma radiation. A highly anisotropic mosaic-block orientation was found. The ensuing anisotropy in secondary extinction could be fairly well described by the Thornley-Nelmes formalism, with adjusted mosaicities close to the directly observed ones. The structure factors have been analyzed by a multipole expansion model within the Hartree-Fock framework. Thermal mean-square atomic amplitudes are distinctly different along the a and c axes. The total $3d$ charge exhibits appreciable anisotropy with an excess of density in the singlet a_g along the c axis and a deficiency in the two doublet e_g orbitals. The $3d$ shell in the metal shows a slight contraction of 1.2% relative to the free atom. Agreement with low-order form factors from critical-voltage electron diffraction reaches 0.1%. No difference of d-electron count is found between metal and atom. A $3d^7$ configuration implies incomplete filling of the majority-spin band. The directed metallic bonds are characterized in terms of the electron density topology.

DOI: 10.1103/PhysRevB.80.125126 PACS number(s): 61.05.cp, 71.20.Be, 61.66.Bi

I. INTRODUCTION

Gamma-ray single-crystal diffraction has recently been employed in a number of comprehensive electron density studies of $3d$ transition metals with cubic crystal structures such as chromium,[1] iron,[2] and nickel.[3] The present work extends these studies to the case of hexagonal cobalt.

For heavier elements with increasing core-electron density, accessibility of highly accurate crystal structure factors is a crucial requirement for a reliable determination of the redistribution of valence electrons in the solid. Standard x-ray diffraction techniques are of little help in tackling such problems. Enhanced accuracy is offered by the use of 316.5 keV gamma radiation. Besides the high energy, favorable properties comprise the perfect stability, homogeneity, and monochromaticity ($\Delta\lambda/\lambda=10^{-6}$) of the incident γ-ray beam.

So far, there is no experimental information on the distribution of electron charge density in the unit cell of cobalt metal, neither could we find an experimental or theoretical Debye-Waller factor in the literature. In view of its prominent position, forming one of the three ferromagnetic elements, there is a need to fill this gap.

II. DATA COLLECTION AND REDUCTION

At ambient conditions, the stable phase of cobalt metal has a hexagonal close-packed (hcp) structure (space group $P6_3/mmc$) with atoms at $\frac{1}{3},\frac{2}{3},\frac{1}{4}$ and $\frac{2}{3},\frac{1}{3},\frac{3}{4}$. The site symmetry at these positions is $\bar{6}m2$. The lattice constants are $a=2.5071$ Å, $c=4.0695$ Å at 295 K.[4] The axial ratio $c/a=1.623$ is slightly less than the value 1.633 for ideal hexagonal closest packing of spheres. It means that the nearest-neighbor distance between atoms in adjacent layers (2.496 Å) is 0.5% shorter than that between atoms in the same layer (2.507 Å). The single crystal used in the present investigation was a cube of dimensions $2.45\times2.47\times2.49$ mm^3 purchased from MaTecK/Jülich (Germany).

Double-crystal γ-ray diffraction (angular resolution: 1.5 s of arc) was employed to map the 100, 010, and 110 rocking curves, which revealed perfect Lorentzian peak shapes with a fitted full width at half maximum (FWHM) of 1.40(2), 1.33(2), and 1.15(2) min of arc, respectively. The FWHM of 002 was much broader, namely, 7.28(5) min of arc. The width of general hkl reflections varied linearly with the diffractometer inclination angle χ between the two extremes, $hk0$ ($\chi=0°$) and $00l$ ($\chi=90°$). The anisotropy of the mosaic-spread distribution will be accompanied by anisotropic secondary extinction in the sample.

The diffraction data have been collected on the four-circle gamma-ray diffractometer installed at the Helmholtz-Zentrum Berlin, where the most intense line of a ^{192}Ir source ($T_{1/2}=73.83$ d) with a wavelength of 0.0392 Å (316.5 keV) is used. Important experimental details are summarized in Table I. For practical reasons, the very weakest reflections were not measured. Up to $\sin\theta/\lambda=1.8$ Å^{-1}, completeness of the data is 78%. Since the absorption-weighted mean path lengths varied by 10%, symmetry-equivalent reflections were not averaged. Data reduction was carried out using the XTAL suite of programs.[6]

A possible source of experimental error arises from multiple diffraction (Renninger effect). Any multiple diffraction peak requires a particular sample orientation. By slightly rotating the crystal around the scattering vector, the multiple diffraction conditions vary rapidly, while single diffraction is unaffected. The six strongest reflections, including up to six equivalents, were examined at three different azimuthal settings ψ. Significant intensity diminution was observed in a few cases, and the corresponding data were removed.

The inelastic thermal diffuse scattering (TDS) component from acoustic phonons, lying beneath the Bragg peaks, was

TABLE I. Experimental details. The linear absorption coefficient μ is obtained from Ref. 5. $\overline{T_\mu}$ denotes the absorption-weighted mean path length through the crystal.

Temperature (K)	295 (ambient)
Wavelength (Å)	0.0392
μ (cm^{-1})	0.939
Transmission range	0.796–0.811
$\overline{T_\mu}$ range (mm)	2.210–2.432
Reflections used	419
Independent reflections	181
$(\sin\theta/\lambda)_{max}$ ($Å^{-1}$)	1.893
Overall counting-statistical $\Sigma\sigma(I)/\Sigma I$	0.0065

subtracted according to the formalism of Skelton and Katz.[7] The sound velocities were taken from Ref. 8. The maximum correction factor was $\alpha=I_{TDS}/I_{Bragg}=0.24$ for the 0,0,14 reflection with its increased peak width.

III. DATA ANALYSIS

Refinements were carried out with the program VALRAY,[9] minimizing $\chi^2=\Sigma w(|F_o|^2-|F_c|^2)^2$, where F_o and F_c are the observed and calculated structure factors, respectively. The weights, $w=1/\sigma^2(|F_o|^2)$, are solely based on the counting-statistical variances.

The valence electron configuration of the free cobalt atom $3d^7 4s^2$ ($^4F_{9/2}$) was applied, with the scattering factors calculated from the Hartree-Fock functions tabulated by Clementi and Roetti.[10] Refinements using the $3d^8 4s^1$ configuration showed much worse agreement indices and will be considered in Sec. IV D.

A. Scale factor

Since the structure factors are measured on a relative rather than an absolute scale, a scale factor k defined by $k^{-1}|F_o|=|F_c|$ has to be established by reference to a set of calculated theoretical structure factors. Its estimate is dependent on the quality of the scattering model.

Spherical-atom refinements based only on high-order reflections strongly reduce the influence of deformations in the outer shell. The threshold for $\sin\theta/\lambda$ should be as large as possible. On the other hand, the high-order data set should be large enough to reduce the correlation between thermal parameters and k. From several cut-off values, $\sin\theta/\lambda=0.7$ $Å^{-1}$ was chosen as adequate, with the least-squares fit yielding $k=1.0044(10)$ [correlation coefficient $\mathrm{corr}(k,U_{11})=0.85$]. From the observed mosaicity, it is predicted that there are still noticeable contributions from extinction ($y=I_{obs}/I_{kin}\geq 0.992$, where I_{obs} and I_{kin} are the observed and kinematic intensities), which have been accounted for.

It is also possible to obtain k by scaling on the calculated structure factors for a more flexible multipole model (see below), now using all data. Trial values of k are chosen and χ^2 is minimized at each point with respect to all other parameters, except for the extinction parameters, which are fixed at the observed values. An increase from the minimum by $\Delta\chi^2=1$ corresponds to a one-standard-deviation departure from the least-squares estimate. The result is $k=1.0013(3)$. There is thus agreement between both scaling procedures, giving confidence in the estimate of the very narrow statistical error.

The observed structure factor contains a contribution from the nuclear Thomson scattering amplitude. The value for cobalt $f_N=0.0068$ electron units is negligible for the present data set, which does not reach the extreme accuracy level of the previous one for Ni.

B. Multipole model

The electron density is represented as a nucleus-centered expansion of real spherical harmonics.[11] In the case of hcp Co, its analytical representation consists of the spherical core and $4s$ electrons, as well as the spherical and aspherical parts of the $3d$ valence shell,

$$\rho_{Co}(\mathbf{r}) = \rho_{core}(r) + \rho_{4s}(r) + \kappa^3\rho_{3d}(\kappa r) + P_2\kappa^3\rho_2(\kappa r)y_{20}(\mathbf{r}/r) + P_4\kappa^3\rho_4(\kappa r)y_{40}(\mathbf{r}/r).$$

Only even-order spherical harmonics ($l=0,2,4$) contribute to a d-orbital density, so that for site symmetry $\bar{6}m2$ the allowed higher poles are y_{20} and y_{40}.

ρ_{core}, ρ_{4s}, and ρ_{3d} are Hartree-Fock densities of the appropriate atomic orbitals.[10] The radial function of the quadrupole and the hexadecapole is constructed from a $3d3d$ atomic-orbital product. The population coefficients P_2, P_4, and the radial expansion-contraction factor κ are variable parameters. The Cartesian frame is oriented with $x\|\mathbf{a}$, $y\|\mathbf{c}\times\mathbf{a}$, and $z\|\mathbf{c}$.

C. Anisotropic extinction

Since the mosaic misorientation about the hexagonal growth axis of the crystal is much larger than perpendicular to it, extinction has to be treated anisotropically. The mosaic-spread distribution is taken of the tensorial form proposed by Thornley and Nelmes.[12] In the present case, the second-rank mosaic tensor has the point symmetry of the crystal, so that the number of independent elements reduces from six to two. The value for the extinction correction for a given reflection depends upon a characteristic vector, defining the orientation of the crystal with respect to the diffraction plane.

The secondary extinction parameters were adjusted together with all other parameters. The result for the Lorentzian (FWHM) principal axes is $\eta_1=1.06(3)$ and $\eta_3=9.5(4)$ min of arc. Though the agreement between the mosaic spreads obtained from the refinement and the ones observed from profile measurements is not perfect, the anisotropic model provides physically pertinent values. It should be emphasized that the extinction effects were not severe. The maximum reduction in $|F_o|^2$ is 8.4%, and a total of four independent reflections have an extinction reduction up to 6%. The maximum difference in the calculated reduction factor, arising from the discrepancy between observed and fitted mosaic widths, is 0.5%.

TABLE II. Mean-square vibrational amplitudes and multipole model parameters of cobalt at room temperature. U_a and U_c are the components along the a and c axes. Reliability factors for the 419 observations: $R(F)=\Sigma|F_o-F_c|/\Sigma|F_o|=0.0064$, $wR(F^2)=[\Sigma w(F_o^2-F_c^2)^2/\Sigma wF_o^4]^{1/2}=0.0100$. Reduced chi-square: $\chi^2/(\text{degrees of freedom})=1642.5/(419-7)=3.987$.

U_a (Å^2)	0.00481(1)
U_c (Å^2)	0.00532(3)
κ	1.0122(16)
P_2 ($\|e\|$Å^2)	0.430(33)
P_4 ($\|e\|$Å^4)	0.339(21)

IV. RESULTS AND DISCUSSION

Final parameters and statistical indicators for the multipole refinement are given in Table II. The data clearly support the applied model, as indicated by the narrow confidence limits of the fit parameters. Though the actual value of χ^2 is considerably larger than the ideal one, the fit residuals are evenly distributed, and no systematic trends are encountered. The distribution of the residuals is heavier tailed than a Gaussian (10% of the data points deviate between 3 and 5.5σ). In the following, physical implications of the deduced parameters will be examined.

A. Atomic vibrational amplitudes

There is an appreciable anisotropy in the mean-square amplitudes of vibration. The vibrations along the hexagonal axis are larger than in the basal plane $U_c/U_a=1.106(6)$. As noted in the introduction, owing to a lack of available data, no comparison can be made with other results. It has been pointed out that there should be a correlation between the anisotropy ratio and the axial ratio c/a for the hcp elements.[13] Mg has the same axial ratio as Co, $c/a=1.623$, and its U_c/U_a value is indeed also found to be larger than one.[13]

The possible influence of anharmonic contributions to the Debye-Waller factor has been investigated. For point symmetry $\bar{6}m2$, there are one third- and three fourth-order terms allowed in the Gram-Charlier expansion of the atomic probability function. In view of the insignificant improvement of fit ($\Delta\chi^2=-0.9\%$), one may safely assume that the nuclear motion is in a harmonic potential.

B. Asphericity of charge distribution

In a hexagonal environment, the atomic d orbitals split into two doublets e_g, e_g', and a singlet a_g. With the quantization axis z along the c direction, the singlet corresponds to d_{z^2}, $a_g(z^2)$, whereas the doublets $e_g(xz,yz)$, $e_g'(xy,x^2-y^2)$ are composed of d_{xz}, d_{yz} and d_{xy}, $d_{x^2-y^2}$, respectively. A detailed discussion of the d-orbital analysis for trigonal symmetry (including the corrected orbital-multipole matrix) is given in Ref. 14 and will not be repeated here.

The orbital occupancies determined from the multipole population parameters are $P(a_g)=1.846(22)$, $P(e_g')=2.567(19)$, and $P(e_g)=2.587(16)$ electrons. For spherical symmetry, the relative occupancies are 40% (e_g'), 40% (e_g), and 20% (a_g). The experimental result reveals distinct anisotropy with 37% (e_g'), 37% (e_g), and 26% (a_g). The a_g orbital is thus populated in excess, whereas the e_g orbitals are depopulated relative to the free atom. The orbital occupancies are clearly reflected in Fig. 1, which shows the static model deformation density (aspherical components only) in the (110) plane and in the hexagonal plane. The dominant feature is electron buildup in the two a_g lobes aligned along [001]. The pattern in the hexagonal plane comes from the central ring of the cylindrical a_g orbitals.

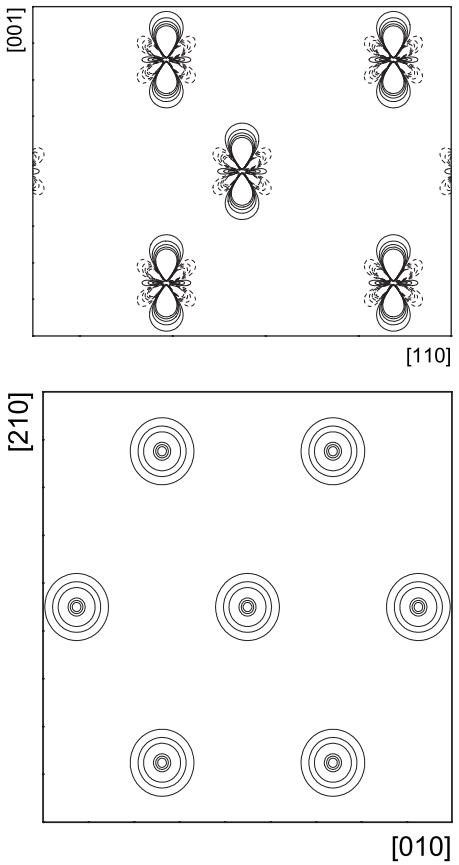

FIG. 1. Aspherical contributions to the static model density. Top: (110) plane (8×6 Å^2) with a density range from -1.22 to $4.76e$ Å^{-3}; more than one unit cell is shown to illustrate the *ABAB*… stacking along the c axis. Bottom: basal plane of the hcp structure (6×6 Å^2) with a density range from 0 to $0.37e$ Å^{-3}; the full hexagonal surrounding of one Co atom is displayed. Solid lines represent regions of excessive density and dashed lines represent depleted regions in steps of $0.1e$ Å^{-3}. The zero contour is omitted. The densities are truncated at $\pm0.5e$ Å^{-3}.

Symmetry allows also the odd order deformation function y_{33-} which, when introduced into the model in the form of a $3p3d$ orbital product, leads to a virtually zero population.

C. X-ray radial 3*d* form factor

The $3d^7$ valence shell exhibits a small spatial contraction of 1.2% relative to the free atom. A comparison of our results for the $3d$ radial extent in transition metals is given in Table III. In all cases, a spatially more compact distribution

TABLE III. Refined radial contraction relative to the independent-atom $\langle r\rangle_{3d}$ value.

	bcc Cr	bcc Fe	hcp Co	fcc Ni
Contraction (%)	12.6(2)	8.9(2)	1.22(16)	2.07(5)

is found in the solid, strongly supporting a localized atomic character of the 3*d* electrons. The conflicting aspects between itinerant and localized electron models are still an essential issue of present-day interest. Concerning the degree of spatial contraction, it will be noticed from Table III that there appears to be a substantial difference between body-centered and close-packed structures.

For a hcp lattice, the atomic form factor f_{hkl} is related to the fitted structure factor F_{hkl} through $F_{hkl}=C_{hkl}f_{hkl}T_{hkl}$, where $C_{hkl}=2\cos\{[2\pi(h+2k)/3+l/4]\}$ equals 2, $\sqrt{3}$, or 1 for the three symmetry-allowed sets of reflections, and the temperature factor can be written as $T_{hkl}=\exp[-(h^2+hk+k^2)\beta_a-l^2\beta_c]$ with $\beta_a=8\pi^2U_a/(3a^2)$ and $\beta_c=2\pi^2U_c/c^2$. In Table IV, absolute values of the crystal scattering factor are listed for 20 diffraction vectors, where also the numerical contributions of both the core and valence electrons have been individually identified. As seen from the table, the difference between the metallic form factor and the atomic one is very small.

A band-structure calculation for ferromagnetic hcp cobalt was performed by Matsumoto *et al.*,[15] who also presented selected theoretical x-ray form factors. In Table IV, it is shown that the theoretical values are consistently lower by about 1% than the model fit values.

Experimental information to compare with comes from high-energy electron-diffraction measurements. The critical-voltage effect was used to deduce three low-order form factors of hcp Co: $f(002)=19.461$, $f(110)=14.903$, and $f(103)=13.879$.[16] No individual error estimates have been given, rather the general accuracy level is claimed to be ~0.1%. For 002 and 110, the deviations from the γ-ray values are as small as 0.1% and 0.2%. But for 103, the deviation is 1.2%. The discrepancy may be attributed to insufficient knowledge of the temperature factor assumed to be isotropic in the electron-diffraction study. The value used, $U=0.00494$ Å^2, is missing in the quoted reference and could not be found in the literature. Accuracy of the critical-voltage method is limited by errors in the Debye-Waller factor for the higher-order reflections. The interexperiment comparison also sheds light on the reliability of the extinction correction. In the present work, the extinction factors of the three reflections under discussion are $y(002)=0.933$, $y(110)=0.929$, and $y(103)=0.984$. Note that 002 and 110 correspond to the maximum and minimum values of the observed mosaic spread. The excellent agreement found for the corresponding form factors clearly supports the validity of the Thornley-Nelmes description of anisotropic extinction.

D. Number of 3*d* electrons

In the metal, the number of 3*d* electrons may be different from that in the free atom. Assuming the electron configuration $3d^84s^1$ ($^4F_{9/2}$) with Hartree-Fock wave functions from Clementi and Roetti[10] results in an increase in χ^2 by $\Delta\chi^2=45\%$ relative to the atomic ground-state configuration

TABLE IV. Static scattering factors from the multipole model fit for metallic cobalt in units of *e*/atom. f_{core} and $f_{valence}$ denote the contributions from the core (including 4*s*) and $3d^7$ valence electrons, respectively. f is the total contribution from all electrons. f_{atom} is calculated from Ref. 11 for a $3d^74s^2$ independent atom, and f_{theory} is taken from Ref. 15.

hkl	sin θ/λ (Å^{-1})	f_{core}	$f_{valence}$	f	f/f_{atom}	f/f_{theory}
100	0.2303	15.654	4.492	20.146	1.005	1.014
002	0.2459	15.370	4.112	19.483	0.998	1.007
101	0.2610	15.096	3.967	19.063	1.003	1.011
110	0.3989	12.627	2.242	14.869	1.010	1.016
103	0.4348	12.016	1.697	13.713	0.997	1.001
200	0.4606	11.593	1.663	13.256	1.012	1.015
104	0.5430	10.366	0.899	11.265	0.997	0.999
120	0.6093	9.532	0.746	10.279	1.014	1.014
300	0.6909	8.693	0.453	9.146	1.014	1.014
302	0.7333	8.329	0.276	8.605	1.007	1.006
006	0.7376	8.295	0.256	8.551	1.005	1.006
220	0.7977	7.857	0.213	8.070	1.014	1.014
130	0.8303	7.649	0.164	7.812	1.014	1.015
222	0.8348	7.622	0.108	7.730	1.007	1.008
116	0.8385	7.600	0.015	7.615	0.996	0.996
304	0.8480	7.544	0.002	7.546	0.995	0.996
400	0.9211	7.154	−0.065	7.089	0.995	0.997
224	0.9371	7.078	−0.064	7.014	0.996	0.998

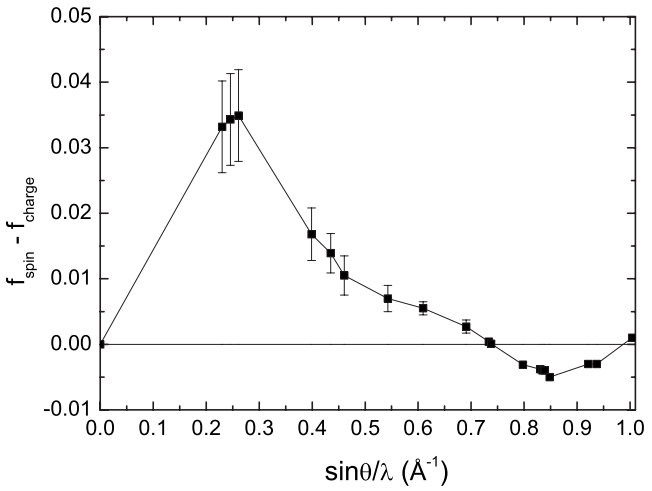

FIG. 2. The difference between the spherically symmetric spin form factor (Ref. 20) and the radial charge form factor for $3d^7$ ($\kappa = 1.0122$) as deduced from neutron and γ-ray diffraction. The form factors are normalized to unity at $\sin\theta/\lambda = 0$.

$3d^7 4s^2$. A clear choice in favor of d^7 can thus be made on the value of the χ^2 statistic alone. It is the lowest-order Bragg reflection 100, which is most sensitive to the d electron count. In the case of bcc iron and fcc nickel, the situation was quite different, as the χ^2 values happened to be much closer for the two $3d$ configurations in question. The decision for Fe($3d^7 4s^1$) and Ni($3d^8 4s^2$) was based on additional physical information. It is tempting to conjecture a marked difference between body-centered and close-packed structures concerning the occupation of $3d$ and/or $4s$ orbitals. A comparative study of bcc vanadium would be of interest.

Further insight into the electronic structure of hcp Co is obtained by observing that the d-shell contribution to the spin magnetic moment is $\sim 1.5\mu_B$ per atom, with close agreement between experimental values and density-functional-based calculations.[17] A d^7 configuration is thus incompatible with a fully occupied majority-spin band. The consistent numbers of majority-and minority-spin are $n(\alpha) = 4.25$ and $n(\beta) = 2.75$. Complete subband filling would require $8.5d$ electrons per atom. It should be noted that hcp Co is traditionally classified as a strong ferromagnet, which is defined by one spin band being fully occupied, contrary to a weak ferromagnet where both majority- and minority-spin d states are only partially occupied. Total $3d$ occupation numbers of 7.45 and 7.57 have been reported from first-principle calculations.[18]

E. Magnetic form factor

The magnetic form factor of hexagonal cobalt was determined by Moon in 1964 using polarized neutron diffraction.[19] The most remarkable finding was the nearly ideal spherical symmetry of the unpaired $3d$ electron distribution.

For an atom with unbalanced net spin, the unequal α-α and β-β exchange interactions cause the spatial orbitals of the majority α-spin electrons to be contracted relative to the β-spin counterparts $\langle r(\alpha)\rangle < \langle r(\beta)\rangle$. The radial part of the magnetic form factor f_{spin} is therefore expected to show a small but significant difference from the radial charge form factor f_{charge}. From Fig. 2, it is seen that the integral over the difference $f_{spin} - f_{charge}$ has a positive value. This finding is most clearly understood via the Silverman-Obata sum rule,[21] which connects the spherical form factor with the average value of r^{-1}: $\int_0^\infty f(q)dq = \frac{\pi}{2}\langle r^{-1}\rangle$. The inequality $\langle r^{-1}\rangle_{spin} > \langle r^{-1}\rangle_{charge}$ predicted from the unrestricted open-shell Hartree-Fock formalism is thus satisfied for the Co($3d^7$) configuration.

F. 4*s* electrons

The $4s$ electrons have a diffuse distribution of average radius $\langle r\rangle = 1.67$ Å, and the form factor goes through zero at $\sin\theta/\lambda = 0.2$ Å^{-1} followed by small negative values between 0.2 and 0.4 Å^{-1}. Scattering contributions are thus limited to the three innermost reflections. Their sensitivity with respect to a $4s$ charge rearrangement has been examined. A deterioration of χ^2 by 7% occurs for $3d^7 4s^0$ relative to $3d^7 4s^2$. From the two extreme cases, free-electron and atomic-like behavior, the latter is favored by the diffraction data. Joint refinement of a radial scaling parameter $\kappa'(4s)$ and a population parameter of the form $3d^{7+n}\ 4s^{2-n}$ substantiates the independent-atom values $\kappa' = 1.035(27)$ and $n = -0.078(51)$. The valence density thus evidences significant $4s$ character, demonstrating that the assumption of free electrons is oversimplifying the actual situation in transition metals. In the interatomic region, the $4s^2$ density has a constant value of $\sim 0.2e$ Å^{-3}, now characteristic for two freely moving electrons.

G. Topological features

Topological features of the electron density provide insight into bonding interactions in terms of the critical points ($\nabla\rho = 0$) and the Laplacian $\nabla^2\rho$.[22] Besides maxima (3,−3) and minima (3,3), there are two types of saddle points (3,1)

TABLE V. Characteristics of the bond critical points. $\lambda_\parallel$ denotes the curvature of $\rho(\mathbf{r}_c)$ along the internuclear line. Values of ρ in e Å^{-3}, values of $\nabla^2\rho$, and $\lambda_\parallel$ in e Å^{-5}. The kinetic-energy density $G(\mathbf{r}_c)$ and the potential-energy density $V(\mathbf{r}_c)$ are calculated from the Abramov functional (Ref. 25) and the local virial theorem. G, V, and G/ρ are given in atomic units.

Bond CP	$\rho(\mathbf{r}_c)$	$\nabla^2\rho(\mathbf{r}_c)$	$\lambda_\parallel$	$G(\mathbf{r}_c)$	$V(\mathbf{r}_c)$	$G(\mathbf{r}_c)/\rho(\mathbf{r}_c)$
Basal plane	0.286	1.90	2.73	0.0279	−0.0361	0.658
Out of plane	0.288	2.02	2.82	0.0289	−0.0369	0.678

and (3,−1). In the (*rank*, *signature*) convention, rank is the number of nonzero eigenvalues, and signature is the sum of the signs of the eigenvalues of the Hessian matrix. In particular, (3,−3) corresponds to an atomic site, and the properties at the (3,−1) saddle point between two nuclei, called bond critical point, sum up very concisely the nature of the interaction between the connected atoms.

The following critical-point network was revealed: (3,−3) at 2*c*, (3,−1) at 6*g* and 6*h*, (3,1) at 2*b*, 2*d* and 12*k*, and (3,3) at 2*a* and 4*f* positions. The number of critical points of each kind within the crystal unit cell is connected by the Poincaré-Hopf relation: $n(3,-3)+n(3,1)=n(3,3)+n(3,-1)$.[23] The above set satisfies the relation and is thus consistent. The existence of maxima in electron density at non-nuclear positions in elemental metals (e.g., hcp beryllium and magnesium) has been a subject of controversy for some time.[24] No non-nuclear (3,−3) critical point is found for hcp cobalt.

Every atom in the basal plane is bound to six atoms in the same plane. In addition, six bonds are directed toward the nearest-neighbor atoms above and below the basal plane. Characteristics of the bond critical points are presented in Table V. Typical features of metallic bonds are manifested, such as low values of $\rho(\mathbf{r}_c)$, positive Laplacians, and a low kinetic energy per electron $G(\mathbf{r}_c)/\rho(\mathbf{r}_c)<1$ (in atomic units). The results for hcp Co invite for a comparison with the related cubic transition metals (see Table 5 in Ref. 3). Despite the very different global topologies of the charge density, the local bond properties are quite similar, independent of lattice type or number of 3*d* electrons. The investigated compounds, however, share one essential feature, that is, almost equal interatomic distances of ~2.5 Å. The distance in bcc vanadium is 2.62 Å, so that different critical parameters should be encountered if mere proximity of atoms is the influencing factor.

V. CONCLUDING REMARKS

The electron density distribution of ferromagnetic hcp cobalt was studied here. Important findings may be summarized as follows: (i) the Thornley-Nelmes representation of the anisotropic mosaic distribution gives a good account of anisotropy in secondary extinction as validated by comparison between refined and directly observed mosaicities; (ii) close accordance is found with low-order structure factors from electron-diffraction measurements on an absolute scale; (iii) there is distinct charge asphericity showing a preference for a_g orbital occupancy; (iv) the 3*d* shell is slightly contracted relative to the free atom; (v) the metallic configuration is approximately d^7 rather than d^8; (vi) the majority-spin *d* band is not completely filled; and (vii) a localized valence electron model is supported.

ACKNOWLEDGMENTS

We thank H.-J. Bleif for helpful discussions. Support from the Deutsche Forschungsgemeinschaft (Grant No. UL164/4) is acknowledged.

[1] W. Jauch and M. Reehuis, Phys. Rev. B **73**, 085102 (2006).
[2] W. Jauch and M. Reehuis, Phys. Rev. B **76**, 235121 (2007).
[3] W. Jauch and M. Reehuis, Phys. Rev. B **78**, 235113 (2008).
[4] F. Vincent and F. Figlarz, C. R. Hebd. Séances Acad. Sci. **264C**, 1270 (1967).
[5] J. H. Hubbell and S. M. Seltzer, National Institute of Standards and Technology Internal Report 5632, 1995; also available via http://www.physics.nist.gov/PhysRefData/XrayMassCoef/cover.html
[6] *Computer Code XTAL 3.4, User's Manual*, edited by S. R. Hall, G. S. D. King, and J. M. Stewart (University of Western Ausralia, Perth, Australia, 1995).
[7] E. F. Skelton and J. L. Katz, Acta Crystallogr., Sect. A: Cryst. Phys., Diffr., Theor. Gen. Crystallogr. **25**, 319 (1969).
[8] D. Antonangeli, M. Krisch, G. Fiquet, J. Badro, D. L. Farber, A. Bossak, and S. Merkel, Phys. Rev. B **72**, 134303 (2005).
[9] R. F. Stewart, M. Spackman, and C. Flensburg, *Computer Code VALRAY, User's Manual* (Carnegie-Mellon University, Pittsburgh, Pennsylvania/University of Copenhagen, Copenhagen, Denmark, 2000).
[10] E. Clementi and C. Roetti, At. Data Nucl. Data Tables **14**, 177 (1974).
[11] R. F. Stewart, Acta Crystallogr., Sect. A: Cryst. Phys., Diffr., Theor. Gen. Crystallogr. **32**, 565 (1976).
[12] F. R. Thornley and R. J. Nelmes, Acta Crystallogr., Sect. A: Cryst. Phys., Diffr., Theor. Gen. Crystallogr. **30**, 748 (1974).
[13] Y. Watanabe, H. Iwasaki, and S. Ogawa, Jpn. J. Appl. Phys. **10**, 786 (1971).
[14] W. Jauch and M. Reehuis, Phys. Rev. B **67**, 184420 (2003).
[15] M. Matsumoto, M. Tokii, and S. Wakoh, J. Phys. Soc. Jpn. **67**, 4291 (1998).
[16] A. G. Fox and R. M. Fisher, Aust. J. Phys. **41**, 461 (1988).
[17] S. Chadov, J. Minár, M. I. Katsnelson, H. Ebert, D. Ködderitzsch, and A. I. Lichtenstein, EPL **82**, 37001 (2008).
[18] B. I. Min, T. Oguchi, and A. J. Freeman, Phys. Rev. B **33**, 7852 (1986); R. Wu and A. J. Freeman, Phys. Rev. Lett. **73**, 1994 (1994).
[19] R. M. Moon, Phys. Rev. **136**, A195 (1964).
[20] R. M. Moon, Int. J. Magn. **1**, 219 (1971).
[21] J. N. Silverman and Y. Obata, J. Chem. Phys. **38**, 1254 (1963).
[22] R. F. W. Bader, *Atoms in Molecules: A Quantum Theory* (Clarendon, Oxford, 1990).
[23] P. F. Zou and R. W. F. Bader, Acta Crystallogr., Sect. A: Found. Crystallogr. **50**, 714 (1994).
[24] J. Friis, G. K. H. Madsen, F. K. Larsen, B. Jiang, K. Marthinsen, and R. Holmestad, J. Chem. Phys. **119**, 11359 (2003).
[25] Yu. A. Abramov, Acta Crystallogr., Sect. A: Found. Crystallogr. **53**, 264 (1997).